

UC Santa Barbara

UC Santa Barbara Previously Published Works

Title

On localization performance in imaging sensor nets

Permalink

<https://escholarship.org/uc/item/5fs7w22v>

Journal

IEEE Transactions on Signal Processing, 55(10)

ISSN

1053-587X

Authors

Ananthasubramaniam, Bharath

Madhow, Upamanyu

Publication Date

2007-10-01

DOI

10.1109/TSP.2007.896260

Peer reviewed

On Localization Performance in Imaging Sensor Nets

Bharath Ananthasubramaniam, *Student Member, IEEE*, and Upamanyu Madhow, *Fellow, IEEE*

Abstract—We propose a massively scalable “imaging” architecture for sensor networks, in which sensor nodes act as “pixels” that electronically reflect (and possibly modulate data on top of) a beacon transmitted by a collector node. The collector employs sophisticated radar and image processing techniques to localize the responding sensor nodes, and (if data modulation is present) multiuser data demodulation techniques to extract the data sent by multiple sensors. The sensors do not need to know their own locations, do not need to communicate with each other, and can be randomly deployed. In this initial exposition, we develop basic insight into the localization capabilities of this approach, ignoring sensor data modulation. This reduces to an idealized one-bit, on-off keyed, communication model in which the sensors are either “active” or “inactive,” with the active sensors responding to the collector’s beacon without superimposing data modulation. We consider a moving collector, with the sensor reflections creating a synthetic aperture radar (SAR)-like geometry. However, the collector must employ significant modifications to SAR signal processing for estimation of the location of the active sensors: noncoherent techniques similar to those in noncoherent radar tomography to account for the lack of carrier synchronization between sensor and collector nodes, and decision feedback mechanisms for estimation of the locations of multiple closely spaced active sensors. Measures for localization performance are defined, and the effect of system parameters such as bandwidth, beamwidth and signal-to-noise-ratio (SNR) on performance is investigated.

Index Terms—Data collection, imaging sensor nets, localization, sensor network architecture, virtual radar.

I. INTRODUCTION

VERY large-scale sensor networks arise naturally when low-cost microsensors with small sensing range are used to provide coverage of a large area. Such networks have a number of important applications, including border policing, monitoring for biological or chemical agents over large urban areas, and even interplanetary exploration. Key to their utility is the ability to randomly deploy large numbers (hundreds of thousands) of sensor nodes, and to monitor them from afar (e.g., deployment, as well as monitoring might be performed by aircraft or spacecraft). In such settings, the conventional approach of data collection using multihop wireless networking among the sensor nodes is often inapplicable. Specifically, if the collector node is far from the sensor field, then multihop relay

among the sensor nodes leads to negligible reduction of the distance to the collector node. Examples of such applications are data collection from a remote sensor field by aircraft, satellite, or stationary monitoring facilities. Moreover, as shown by the pioneering work of Gupta and Kumar [1], as well as many subsequent analyses of the capacity of multihop networks [2]–[5], multihop networking does not, in general, scale to very large networks, with the throughput per node scaling down with the network size under standard assumptions on network traffic. An equally significant consideration is the overhead of addressing and routing in large networks. Large-scale random deployment also implies that the map between sensor node identity and location is not known *a priori* to either the sensor nodes or the collector node(s). However, since a key component of data collected from a sensor network is the location of interesting events, localization is a must. Conventional solutions such as GPS are often inapplicable due to cost (for truly large-scale deployments, we wish to drive the sensor node cost well below even the dropping price of a GPS receiver) and availability (GPS is easy to jam on Earth, and is not available, say, on the surface of Mars).

In order to simultaneously address the problems of scale and localization, we turn to an analogy with imaging in order to obtain an “Imaging Sensor Net” architecture: the sensor nodes play the role of pixels being “imaged” by a sophisticated data collector node. The sensors electronically reflect the collector’s beacon (and possibly add data modulation to it), thus, creating a *virtual radar* geometry that can be exploited by the collector for fine-grained localization. The collector node can now use radar and image processing algorithms on the received signal to localize the sensor nodes, and multiuser data demodulation techniques to demodulate their data, if any. Since there is no overhead incurred in internetworking the sensor nodes, or in obtaining and conveying location information, the amount of data sent by the sensors can be reduced to a bare minimum (allowing random deployment of “dumb” sensor nodes without geolocation capabilities). Thus, link budgets sufficient for communicating over long distances (up to 100 km, which permits data collection via satellite) can be obtained even with severely energy-constrained sensor nodes.

Contribution and Main Results: Accurate localization of the sensors that detect an event, or have data to report, is an essential feature of an imaging sensor net. Accordingly, we focus on developing fundamental insight into the localization performance achievable in an imaging sensor net, using an idealized model which ignores data modulation. This is a good approximation when low-rate data modulation is imposed on, say, a spread spectrum beacon being reflected by the sensor, as is the case with a prototype which is currently under development [6], [7]. This reduces to a simple one-bit, on-off keyed model for the sensors’ response. Sensors are either “active” or “inactive,” with

Manuscript received November 21, 2005; revised January 8, 2007. The associate editor coordinating the review of this manuscript and approving it for publication was Dr. Venkatesh Saligrama. This work was supported in part by the National Science Foundation by Grants CCF-0431205, ANI-0220118, and CNS-0520335, by the Office of Naval Research by Grants N00014-03-1-0090 and N00014-06-1-0066, and by the Institute for Collaborative Biotechnologies by Grant DAAD19-03-D-0004 from the U.S. Army Research Office.

The authors are with the Department of Electrical and Computer Engineering, University of California, Santa Barbara, CA 93106 USA (e-mail: bharath@ece.ucsb.edu; madhow@ece.ucsb.edu).

Digital Object Identifier 10.1109/TSP.2007.896260

only the active sensors electronically reflecting the collector's RF beacon. We consider a moving collector, with the sensor reflections creating a geometry as in synthetic aperture radar (SAR) [8]–[10]. However, two-dimensional (2-D) matched filtering used in standard SAR processing performs poorly because of the lack of carrier synchronization between the sensor nodes and the collector [11]. Our main results are as follows.

- 1) We provide a maximum likelihood (ML) formulation for localization, considering first an isolated active sensor, which leads to a noncoherent decision statistic based on a simple modification of the 2-D matched filter. The model is similar to that in noncoherent radar tomography [12], [13]. Our ML algorithm also applies to multiple active sensors, provided that they are spaced far enough apart that their 2-D responses at the collector do not overlap.
- 2) Since ML localization for multiple active sensors that are closely spaced is computationally intractable, we develop a suboptimal decision feedback algorithm, in which the estimated response of each active sensor is subtracted out once it is detected. A criterion for terminating the algorithm is provided, based on an analysis of the probabilities of false alarm and miss.
- 3) Key tradeoffs governing localization performance are investigated analytically. Simulation results are provided, and compared with analysis when applicable.

Related Work: Preliminary development of the imaging sensor net paradigm was presented in [11] and [14]. In this paper, we provide a comprehensive treatment of the localization capabilities of this approach. The work that is most closely related to ours is [15], in which sensors are coarsely localized by a collector using a spot beam. However, our objective is to obtain an accurate estimate of the sensors' locations without stringent requirements on the collector's beams.

For more conventional multihop architectures, there has been a great deal of activity in the important problem of localization, broadly classified into two categories. The majority of schemes fall into the first category of *anchor-based* localization [16]–[21], in which a subset of the sensors know their locations, and the information from their beacons is used by other sensor nodes to infer their own locations in an iterative fashion. In the second category of *anchor-free* localization [22], the nodes compute their locations iteratively in a consistent coordinate system. In contrast to the “dumb” nodes in an imaging sensor net, all of the preceding methods require some form of ranging (at different degrees of sophistication) in the sensor nodes, followed by distributed collaborative iterations.

In addition to fundamental research on the capacity of multihop wireless relay mentioned earlier, there is much research aimed at optimizing multihop networks in the specific context of data collection from sensor networks, including routing optimization [23]–[26], distributed source coding [27], [28], and distributed signal processing and estimation [29], [30]. Despite the limits on scalability derived by Gupta and Kumar [1] and others, it is conceivable that in certain settings, the redundancy in the information gathered by the sensor nodes may be such that the net information to be conveyed to a data collection center scales up slowly enough to fit within the Gupta-Kumar bounds [31]. However, as noted earlier, even if the problems of scale

and overhead in multihop networking could be circumvented, it is inapplicable to a large class of applications served by imaging sensor nets, namely, those in which the nodes in the sensor field are more or less at the same distance from the collector node, and all nodes have comparable energy/power constraints.

The system model is presented in Section II. The optimal ML single sensor localization algorithm and a decision-directed joint localization of multiple sensor are developed in Sections III-A and III-B. Noise-limited localization performance, assuming a single active sensor, is considered in Section IV. This is used to get insight into the effect of appropriately chosen dimensionless parameters on performance measures. The performance with multiple active sensors is explored in Section V. Finally, Section VI contains concluding remarks.

II. SYSTEM MODEL

In this section, we describe the system model corresponding to an airborne collector (e.g., an aircraft or UAV), in direct analogy to swath-mode SAR, as shown in Fig. 1(a) and (b). However, these concepts extend directly to other geometries, such as terrestrial vehicles moving along the edge of the sensor field, or stationary collectors with steered beams [32]. The collector node illuminates a part of the field with a beacon using a side-looking antenna. Each such illumination is called a *snapshot*. As seen in Fig. 1(b), the collector moves along one edge of the sensor field at a fixed altitude, and the movement of the collector causes the beacon to sweep the entire field.

Ignoring sensor data modulation, we obtain an idealized one-bit model of the sensor data. Sensors are either “active” or “inactive,” and the objective is to localize the active sensors (i.e., to image the activity in the sensor field). Active sensors that hear the beacon respond to it by transmitting a wideband signal, timing their response precisely with respect to a trigger sequence in the beacon. This creates a SAR-like geometry. The collector node processes the net received signal over multiple snapshots using SAR-like [8]–[10] and noncoherent tomography based [13] techniques to generate an image of the activity in the sensor field. The collector node knows its own location at the time of different snapshots (e.g., an aircraft may know its own GPS location, and its height relative to the sensor field). Thus, the collector can estimate the absolute locations of the active sensors, up to the resolution of this virtual radar system.

A. Received Signal Model

Each active sensor sends back a complex baseband signal, $s(t)$, modulated on a sinusoidal carrier of frequency f_0 . Nevertheless, the techniques in this paper can be easily extended to settings where each active sensor sends back a different signal (e.g., waveforms randomly chosen from a near-orthogonal set) in order to mitigate intersensor interference. The transmitted passband signal is $\tilde{s}(t) = \text{Re}\{s(t)e^{j2\pi f_0 t}\}$. Suppose, there are K active sensors, indexed by k , on the field, and the collector takes J snapshots, indexed by j , of the field. Note that the time reference for each snapshot is different: at each snapshot, at the instant the collector's beacon is transmitted, the time variable is

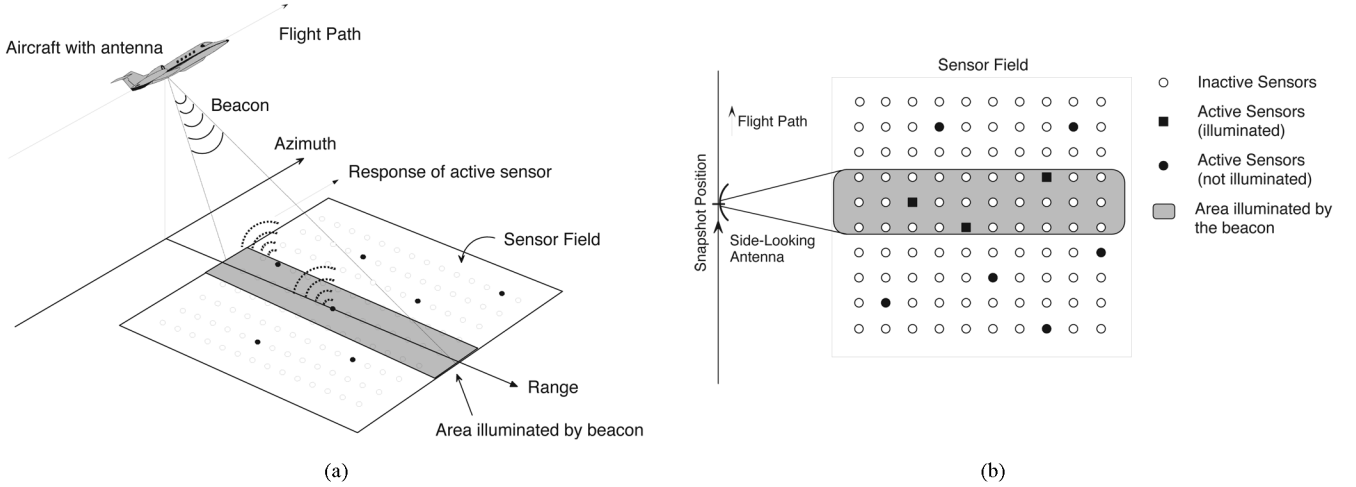


Fig. 1. Imaging sensor net with a moving collector. (a) An aircraft collecting data from a sensor field. (b) Top view of the virtual radar system.

reset to zero to simplify subsequent notation. The complex base-band received signal, $r_j(t)$, at the collector node at snapshot j is

$$r_j(t) = \sum_{k=1}^K h_{j,k} \tilde{I}_{j,k} s(t - \tau_{j,k}) e^{-j2\pi f_0 \tau_{j,k}} + n_j(t), \quad j = 1, \dots, J$$

where $h_{j,k}$ is a complex channel gain, $\tau_{j,k}$ is the round-trip propagation time between active sensor k and the collector node at snapshot j , $\tilde{I}_{j,k}$ is the antenna gain function (AGF) of the collector antenna, which is the antenna gain to sensor k in snapshot j , and $n_j(t)$ is the noise. Note that $r_j(t)$ will be a vector if the collector has multiple receive antennas.

The channel gain, $h_{j,k}$, captures the effects of multipath fading, signal path loss, and lack of synchronization between the local oscillators (LOs) at the sensors and the collector. We assume an additive white Gaussian noise (AWGN) channel with line of sight (LOS) communication. The path loss in the signal is ignored for two reasons: i) the path loss exponent can vary significantly (between 2 and 6) depending on factors such as atmospheric conditions, aperture-medium coupling, frequency of operation, and ii) incorporating this exponent into the estimator does not provide significant improvement in performance, as, in practice, estimates of the exponent are coarse. Since the path loss is ignored, the received signal-to-noise ratio (SNR) is the same for all sensors. Nevertheless, to account for path loss, this SNR can be replaced by the minimum SNR, seen by the farthest sensor, to obtain a conservative estimate of performance. (Fading and shadowing effects, if any, can be accommodated by an outage analysis not undertaken here.)

The LOs at the sensors and the collector are not synchronized. However, the frequency offset between the oscillators is assumed to be small enough that the relative phase is constant over the duration of the transmitted pulse. The relative phases from one snapshot to another are modeled as independent and identically distributed (i.i.d.) over $[0, 2\pi]$. Note that this is a worst case scenario, where no attempt is made to track the frequency drift and phase offset of the sensor LO. Tracking the frequency and phase offsets of the sensor LO provides improved

performance at the cost of more computation at the collector. Under the preceding assumptions, the complex gains for this noncoherent AWGN LOS channel are

$$h_{j,k} = e^{j\theta_{j,k}} \quad k = 1, \dots, K, \quad j = 1, \dots, J$$

where $\theta_{j,k}$ are i.i.d. and uniform over $[0, 2\pi]$. Absorbing all deterministic phases into the random phase factor, the received signal reduces to

$$r_j(t) = \sum_{k=1}^K \tilde{I}_{j,k} s(t - \tau_{j,k}) e^{j\theta_{j,k}} + n_j(t), \quad j = 1, \dots, J. \quad (1)$$

The round-trip delay $\tau_{j,k} = 2R_{j,k}/c$, where $R_{j,k}$ is the distance between the collector node and sensor k in snapshot j , and c is the speed of light. This is identical to conventional radar: the start transmission field reaches active sensor node k at a time $R_{j,k}/c$ after it is generated by the collector node, and the response of sensor k reaches the collector node at a time $R_{j,k}/c$ after it is transmitted by active sensor k .

B. Spatial Coordinate Representation

The received signal model in (1) is used to develop localization algorithms in Section III. It is sometimes convenient to use a spatial received signal representation, to view the sensor field as an ‘image’ or to analyze performance. The y axis of the coordinate system is chosen to be the airborne collector’s flight path. The locations of the K active sensors are $\{(x_k, y_k)\}_{k=1}^K$, and the location of the collector at snapshot j is $(0, z_j = jD)$, where the distance between snapshots is D . The round-trip delay between the sensor and the collector in snapshot j is

$$\begin{aligned} \tau_{j,k} &= \frac{2R_{j,k}}{c} = \frac{2\sqrt{x_k^2 + (y_k - z_j)^2}}{c} \\ &= \frac{2x_k}{c} \sqrt{1 + \frac{(y_k - z_j)^2}{x_k^2}}. \end{aligned}$$

The AGF $\tilde{I}_{j,k} = I(z_j - y_k)$ and the beamwidth of the antenna $2B$ is such that

$$I(y) \leq \epsilon \quad \forall |y| > B \quad (2)$$

for some chosen antenna gain ϵ . Generally, ϵ can be chosen to include the first sidelobes or a significant part of the main lobe. However without any loss of generality in the algorithms in Section III, we assume an antenna with only a main lobe. In practice, an antenna is characterized by an angular beamwidth Θ_{BW} [defined analogously with B in (2)] and B varies with distance from the antenna R as $B = R\Theta_{\text{BW}}$. In this paper, we consider two AGFs: (a) an ideal beam which has unity gain within the beamwidth. Therefore, the AGF $\tilde{I}_{j,k} = 1$ when sensor k is active and is illuminated by the beacon in snapshot j , and 0 otherwise. (b) A more realistic Gaussian beam approximation of a parabolic antenna

$$I(y) = \frac{\sqrt{2}}{\sqrt{\pi}B_{3\text{dB}}} e^{-\frac{2y^2}{B_{3\text{dB}}^2}}, \quad |y| < B$$

where $B_{3\text{dB}}$ is the half-power beamwidth of the antenna ($\epsilon = 0.5$) and $B = B_{3\text{dB}}$. The number of times an active sensor is illuminated by the collector, N , is the ratio of the antenna beamwidth and the distance between snapshots

$$N = \frac{2B}{D}.$$

By the standard far-field approximation employed in SAR, and assuming a highly directional antenna $x_k \gg B$, the round-trip delay can be approximated as

$$\tau_{j,k} \approx \frac{2x_k}{c} = \tau_k \quad (3)$$

observing that only active sensors illuminated by the beacon, satisfying $|y_k - z_j| \leq B$, respond. In other words, a sensor's distance from the collector node is approximated by the 'x' coordinate of the sensor, and sensors at the same range in a given snapshot lie approximately on a line parallel to the y axis. The error due to this approximation is

$$\tau_{j,k} - \tau_k \approx \frac{(y_k - z_j)^2}{cx_k} \leq \frac{B^2}{cx_k} \quad (4)$$

since $|y_k - z_j| \leq B$.

Each sensor is now associated with a single delay τ_k . Hence, (1) becomes

$$r_j(t) = \sum_{k=1}^K \tilde{I}_{j,k} s(t - \tau_k) e^{j\theta_{j,k}} + n_j(t), \quad j = 1, \dots, J. \quad (5)$$

By a coordinate transformation that maps the time-coordinate at each snapshot (recall the time variable is reset at each snapshot) to the 'x' coordinate, and the location of the collector node z_j to the 'y' coordinate, i.e.,

$$t = \frac{2x}{c} \text{ and } z_j = y \quad (6)$$

(5) becomes

$$r(x, y) = \sum_{k=1}^K I(y - y_k) s\left(\frac{2(x - x_k)}{c}\right) e^{j\theta_k(y)} + n(x, y). \quad (7)$$

Note also that the snapshot index j is incorporated into the variable y , i.e., $y = \{jD : j = 1, \dots, J\}$. In practice, the received signal is sampled leading to a received signal matrix, whose rows and columns represent discrete values of 'x' and 'y,' respectively. This provides an elegant way of mapping the entire sensor field to a matrix and to visualize the output of the processing as an image. The received signal representations in (t, j) and (x, y) are equivalent, and either (5) or (7) is used in Section III.

C. Sample Link Budget

We now provide a sample link budget that shows that it is indeed possible to perform virtual radar imaging over significant distances with severely energy-constrained sensor nodes. As in our prototype under development [6], [7], we consider the millimeter wave band, where the small wavelengths allow the generation of highly directional collector beams with antennas of reasonable size. The sensors transmit a 15-MHz PN sequence at 75 GHz (4 mm wavelength) with 500 μW power using an isotropic antenna (0 dB gain). The collector receiver has a high gain (50 dB) parabolic antenna of diameter 0.51 m and noise figure of 3 dB. The total thermal noise power in the signal bandwidth of 15 MHz is -102 dBm. At the nominal range of 3000 m, the received power P_r at the collector can be calculated by Friis' transmission equation as

$$P_r = P_t G_t G_r \left(\frac{\lambda}{4\pi R}\right)^2 \quad (8)$$

where λ is the carrier wavelength, R is the range, P_t is the sensor transmit power, G_t and G_r are the gains of the transmit and receive antennas. The received power P_r per snapshot is calculated to be $0.5 \text{ nW} = -93 \text{ dBm}$. The total noise power added at the receiver per snapshot P_N is the product of the noise and noise figure. Therefore, $P_N = -99 \text{ dBm}$ and $\text{SNR} = P_r/P_N = 6 \text{ dB}$.

For typical parameter values in a SAR-like system considered in this paper, 2 dB SNR suffices to provide good localization performance. Thus, the link budget above provides 4 dB margin, while only requiring 126-nJ energy expenditure per active sensor for 60 snapshots transmitting a 63-chip PN sequence. Sensor nodes that do not have any activity to report can simply turn off their communication circuits in order to conserve energy.

D. Running Example for Simulation Model

Our computer simulations are based on the following running example. The sensor field contains 2500 sensors randomly deployed on a 500 m \times 500 m square grid. Active sensors that detect nearby events are randomly chosen from the deployed sensors while ensuring that there are no edge effects. The

aircraft flies parallel to one side of the field at a distance of 1500 m and an altitude of 2500 m. When illuminated, each active sensor transmits an 11-chip Barker sequence $s(t)$ using a BPSK constellation shaped with a square-root raised cosine pulse with 50% excess bandwidth. The carrier frequency of the sensor transmissions is 75 GHz. The side-looking antenna has a nominal physical beamwidth ($2B$) of 60 m (parabolic antenna diameter of 0.51 m), and the distance between snapshots $D = 1$ m (hence, $N = 60$). The antenna has either an ideal brickwall or Gaussian beam pattern as described in Section II-B. The nominal root-mean-square (rms) bandwidth of the transmitted signal is $\mathcal{W}_{\text{rms}} = 13$ Mhz and receiver sampling rate is 160 MS/s. The SNR at the receiver is defined (in Section II-C) as the ratio of the received power from each sensor to the noise power added at the collector per snapshot, i.e., $\|s\|^2/2\sigma^2$, when the noise is $CN(0, 2\sigma^2)$. Due to oversampling of the received signal, the noise power is appropriately scaled to maintain the correct SNR in the signal band. The nominal operating SNR is 2 dB using the threshold calculated in Section V-A. The normalizing factors for the range and azimuth coordinates to achieve scale invariance are $c/\mathcal{W}_{\text{rms}} = 16.4$ and $D = 1$ m, respectively. The choice and motivation for these normalizing factors are discussed in Section IV-A.

III. IMAGING ALGORITHMS FOR SENSOR LOCALIZATION

Although the virtual radar system geometry is analogous to that of SAR, the standard SAR reconstruction algorithm for sensor localization is inapplicable due to the lack of coherence between the local oscillators at the sensors and the collector. In Section III-A, we present an ML formulation of the problem, assuming a single active sensor, which leads to a noncoherent decision statistic. The ML single sensor algorithm is then used in Section III-B as a building block for a suboptimal decision feedback algorithm for localizing multiple active sensors.

A. Maximum Likelihood Single Sensor Localization

From (5), the received signal in snapshot j due to a single active sensor at $\underline{X} = (x_0, y_0) \equiv (\tau, \{\tilde{I}_j\}_{j=1}^J)$ is

$$r_j(t) = \tilde{I}_j s(t - \tau) e^{j\theta_j} + n_j(t), j = 1, \dots, J \quad (9)$$

where θ_j are i.i.d. uniform random variables, $\tilde{I}_j = I(jD - y_0)$ is the antenna gain to the sensor in snapshot j , and $\tau = 2x_0/c$ is the propagation delay between the sensor and the collector in snapshot j . The received signal vector is

$$\mathbf{r} = \mathbf{s} + \mathbf{n} \quad (10)$$

where

$$\mathbf{r} = \begin{pmatrix} r_1(t) \\ \vdots \\ r_J(t) \end{pmatrix}, \quad \mathbf{s}_j = \tilde{I}_j s(t - \tau) e^{j\theta_j}$$

\mathbf{n} is an AWGN vector, and \mathbf{s} is the active sensor response in the absence of noise.

The location estimate is obtained by maximizing the log-likelihood function, or equivalently, minimizing the Euclidean dis-

tance between the received signal and transmitted signal vectors jointly over \underline{X} and θ_j ,

$$\begin{aligned} \hat{\underline{X}}_{\text{ML}}(y) &= \arg \min_{\underline{X}, \{\theta_j\}} \|\mathbf{r} - \mathbf{s}(\underline{X})\|^2 \\ &= \arg \min_{\underline{X}, \{\theta_j\}} \sum_{j=1}^J \|r_j - \tilde{I}_j s(t - \tau) e^{j\theta_j}\|^2 \\ &= \arg \max_{\underline{X}, \{\theta_j\}} \sum_{j=1}^J \tilde{I}_j |\langle r_j, s(t - \tau) \rangle| \cos(\theta_j - \phi_j) \\ \phi_j &= \text{Arg}\{\langle r_j, s(t - \tau) \rangle\}. \end{aligned} \quad (11)$$

To maximize (11), the $\cos(\theta_j)$ s are replaced by their maximum likelihood estimates, i.e., $\theta_j = \phi_j$. The simplified likelihood function is

$$\hat{\underline{X}} = \arg \max_{\underline{X}} \sum_{j=1}^J \tilde{I}_j |\langle r_j, s(t - \tau) \rangle|. \quad (12)$$

The decision statistic is $\sum_{j=1}^J \tilde{I}_j |\langle r_j, s(t - \tau) \rangle|$, and the sufficient statistic is $\langle r_j, s(t - \tau) \rangle$.

In (11), $\tilde{I}_j = I(jD - y_0)$ is independent of x_0 . However in reality, \tilde{I}_j is a function of x_0 too, due to the broadening of the beam with distance from the antenna described in Section II-B. This dependence does not change the form of (11), and (12) can be modified following the same procedure as

$$\hat{\underline{X}} = \arg \max_{\underline{X}} \sum_{j=1}^J \tilde{I}_j(\tau) |\langle r_j, s(t - \tau) \rangle| - E_s \sum_{j=1}^J \tilde{I}_j(\tau)^2 \quad (13)$$

where $\tilde{I}_j(\tau) = \tilde{I}(jD - y_0, x_0)$ and $E_s = \langle s, s \rangle$. We infer from (13) that the filter used for the azimuth correlation must be varied (lengthened) as a function of the delay τ , which makes the processing more computationally intensive but maintains the simple 2-D filtering structure.

Although a filter matched to $s(t)$ produces the sufficient statistics as in SAR, the optimal processing is nonlinear. The unknown phases, $\{\theta_j\}$, cause the optimal processing to be *non-coherent*, using only the magnitudes of the range correlation for the azimuth processing. These magnitudes are processed using a filter matched to the AGF defined in (2). Thus, a minor modification of the standard SAR algorithm produces the ML-estimation rule for a single active sensor localization. Moreover, if the active sensors are sparsely distributed in the sensor field, then there is no interference between active sensor transmissions. Consequently, the multi-event localization can be performed by repeated application of the single sensor algorithm until all the sensors are detected. A suboptimal algorithm to perform multiple sensor localization, in the presence of interference, is presented in Section III-B.

B. Decision-Directed Joint Localization of Multiple Sensors

The received signal from K active sensors in snapshot j is

$$r_j = \sum_{k=1}^K \tilde{I}_{j,k} s(t - \tau_k) e^{j\theta_{j,k}} + n_j(t), \quad j = 1, \dots, J \quad (14)$$

where $\{\theta_{j,k}\}$ is the set of all unknown random phases at the active sensors. When the active sensors are sparsely distributed on the sensor field with no intersensor interference, the single sensor algorithm in Section III-A is optimal for multisensor ML localization. Two active sensors interfere with each other when their transmissions are overlapping in the 2-D received signal space consisting of one temporal and one spatial dimension (see Section II-A). In the presence of intersensor interference, the optimal ML joint localization algorithm is computationally intractable. Hence, we now present a suboptimal joint detection and localization algorithm that trades off optimality for a lower computational cost.

We adopt a sequential zero-forcing decision-feedback approach where, when an active sensor is detected, it is localized, and the influence of its transmission on the received signal is estimated and subtracted out. This updated received signal is then used to detect (and localize) the next active sensor. The number of active sensors, K , is not known *a priori*, hence, this process is continued until a termination criterion is met.

The sequential detection algorithm is initiated by assuming a single active sensor in the field. The ML localization algorithm for a single sensor is used to obtain an estimate of that sensor's location as

$$\hat{X}_1 = (\hat{\tau}_1, \{\hat{I}_{j,1}\}) = \arg \max_X \sum_{j=1}^J \tilde{I}_j | \langle r_j, s(t - \tau) \rangle | \quad (15)$$

where the estimates $\hat{\tau}$ and $\{\hat{I}_{j,1}\}$ uniquely determine the location of the sensor. Assuming the estimate \hat{X}_1 is the true location, the effect of this active sensor on the received signal is subtracted out. The response of this active sensor also depends on the phases, $\{\theta_{j,1}\}$, for which ML estimates were obtained in (11) as

$$\hat{\theta}_j = \text{Arg}\{\langle r_j, s(t - \tau) \rangle\}.$$

The updated received signal after detecting the first active sensor is

$$r_j^{(1)} = r_j - \hat{I}_{j,1} s(t - \hat{\tau}_1) e^{j\hat{\theta}_j}, \quad j = 1, \dots, J.$$

In general, we denote the updated received signal after detecting k sensors by $r_j^{(k)}$, $k = 0, 1, 2, \dots$, where $r_j^{(0)} = r_j$ is the original received signal. We continue with the detection process after the k th step as long as the following criterion is met:

$$\max_X \sum_{j=1}^J \tilde{I}_j \left| \langle r_j^{(k)}, s(t - \tau) \rangle \right| > T \quad (16)$$

where T is a threshold, whose choice is discussed in Section V-A. If the preceding criterion is satisfied, then the $(k + 1)$ th sensor is localized as follows:

$$\begin{aligned} \hat{X}_{k+1} &= (\hat{\tau}_{k+1}, \{\hat{I}_{j,k+1}\}) \\ &= \arg \max_X \sum_{j=1}^J \tilde{I}_j \left| \langle r_j^{(k)}, s(t - \tau) \rangle \right|. \end{aligned}$$

Violation of the criterion (16) leads to termination of the algorithm. The threshold T is chosen (see Section V-A) such that

the probability of missing a true peak and the probability of false alarms or false peaks under a noise-limited setting meet user-defined tolerances. The algorithm obtained thus is far from optimal and suffers from error propagation, but the alternative of joint ML location estimation is computationally infeasible.

IV. NOISE-LIMITED LOCALIZATION PERFORMANCE

In this section, we focus on noise-limited performance, in order to understand the dependence of the range and azimuth localization resolution on parameters such as SNR, antenna beamwidth, signal bandwidth and antenna beamshape. That is, we analyze the performance of the optimal ML localization algorithm (derived in Section III-A) for a single sensor, ignoring intersensor interference.

A. Scale-Invariant System Dimensions

The description of system dimensions and characterization of system performance in terms of scale-invariant quantities enables prediction of the performance of another system with different physical dimensions, but the same relative dimensions. To this end, we introduce two normalizing parameters or so-called "units" for the range and azimuth directions, respectively. For the range, the reciprocal of the nominal rms signal bandwidth \mathcal{W}_{rms} , expressed as a distance $m_x = c/\mathcal{W}_{\text{rms}}$ where c is the speed of light, is used as the normalizing parameter. For the azimuth $m_y = D$, the distance between successive snapshots, is used. The normalized distances along the x and y coordinates are $X = x/m_x$ and $Y = y/m_y$. The choice of m_x and m_y are based on the resolution analysis in Sections IV-B and IV-C. The simulation results in Section IV-D are presented in terms of these dimensionless quantities.

B. Range Resolution

The analysis of the range resolution using the Cramer-Rao lower bound (CRLB) is only valid when the signal from an active sensor is acquired and the peak is within a half chip length of the actual location. The localization error depends on the distance between the true and estimated locations of the active sensors, and is therefore ill-defined, if the active sensor is not detected, or if there is a false detection. We present in this section a lower bound on the range resolution of the single sensor ML algorithm for an ideal brickwall AGF, under the assumption of sufficiently high SNR such that, the sensor is detected and its transmission acquired within one half-chip interval.

The received signal in (7) from a single active sensor is

$$r(x, y) = I(y - \bar{y})s(x - \bar{x})e^{j\theta} + n(x, y)$$

where n is AWGN, $\theta(y)$ is the random phase, I is the AGF, and $s(x) = s(ct/2)$ is the transmitted signal. We formulate range estimation as a two parameter estimation problem, where the range coordinate \bar{x} and unknown random phase $\theta(y)$ are the parameters estimated. Since the sensor has been detected, $I(y - \bar{y})$ is, or the snapshots with a signal component are known. We use a notation where we drop the independent variables and write the received signal as

$$r = I.s.e^{j\theta} + n$$

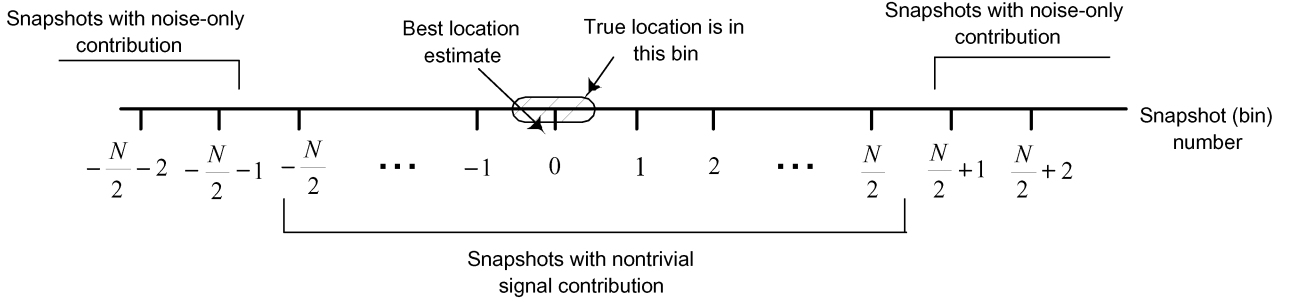


Fig. 2. Random variables and errors in azimuth processing.

and

$$p(r|\bar{x}, \bar{y}, \theta(y)) = \frac{1}{2\pi\sigma^2} e^{-\frac{\|r - I_{se}j\theta\|^2}{2\sigma^2}}.$$

The CRLB for the two parameter estimation, under the condition that both I and s are real, is

$$\begin{pmatrix} \frac{2\sigma^2}{\|I\|^2 \|s'(x)\|^2} & 0 \\ 0 & \frac{2\sigma^2}{\|I\|^2 \|s(x)\|^2} \end{pmatrix}.$$

Defining the rms bandwidth of the signal $s(t)$, and noting that $s'(x) = 2s'(t)/c$

$$W_{\text{rms}}^2 = \frac{\int f^2 |S(f)|^2 df}{\int |S(f)|^2 df} = \frac{\|s'(t)\|^2}{4\pi^2 \|s(t)\|^2} = \frac{c^2 \|s'(x)\|^2}{16\pi^2 \|s(x)\|^2}$$

where $|S(f)|^2$ is the power spectral density of $s(t)$, and c is the speed of light. Observing that $\|I\|^2 = N$ for the ideal AGF, which is the number of times the active sensor is illuminated by the beacon, and that $\|s\|^2/2\sigma^2$ is the transmit SNR per snapshot when $n \sim CN(0, 2\sigma^2)$, the CRLB for the error variance of the range estimate is

$$\sigma_{xx}^2 = \frac{c^2}{16\pi^2 W_{\text{rms}}^2 \text{SNR} N}. \quad (17)$$

The right-hand side (RHS) of (17) has the dimension of c^2/W_{rms}^2 since the other factors are dimensionless. This motivates the choice of $m_x = c/W_{\text{rms}}$ and $X = x/m_x$ in Section IV-A. The error variance of the dimensionless variable X is

$$\sigma_X^2 = \frac{\sigma_{xx}^2 W_{\text{rms}}^2}{c^2} = \frac{W_{\text{rms}}^2}{16\pi^2 W_{\text{rms}}^2 \text{SNR} N}. \quad (18)$$

The use of delay estimation to determine the sensor range in the virtual radar system is evident from the dependence of the performance on the rms signal bandwidth and transmit SNR in (18). The additional factor N accounts for the SNR improvement achieved by averaging out noise in the delay estimates from multiple snapshots, and N . SNR can be regarded as the effective range estimation SNR.

The CRLB provides insight into the tradeoffs between various system parameters by exposing performance trends as a function of these parameters. Since time-delay estimation is asymptotically efficient [33], the CRLB is achievable only at high SNR. However, we do not expect to attain the CRLB even at high SNR, since the CRLB does not account for the far-field

approximation error (4): this is perhaps the most important effect at high SNR. Further, the localization error whose size is measured by the CRLB is not well defined in the event of false alarms and misses, which become more likely at lower SNR.

C. Azimuth Resolution

We next evaluate an upper bound on the azimuth resolution for the ideal brickwall (the performance improves for more realistic Gaussian shaped beams, as shown in the numerical results later in this section). The azimuth estimate is quantized into bins whose size equals the distance D between snapshots, so that there is an irreducible quantization error taking values in $[-D/2, D/2]$. In addition, there are errors that can result from the choice of the wrong bin. In this analysis, we focus on characterizing the latter. For convenience, we label the correct bin as bin 0, as shown in Fig. 2. We also assume that the range uncertainty has been resolved exactly, and that the active sensor has been detected (otherwise the localization error cannot be defined).

We define the *snapshot statistic* for snapshot l as

$$Z_l = \left| \int r_l(t) s(t - \tau) dt \right| \quad (19)$$

where τ is the true round-trip delay and $r_l(t)$ is the received signal corresponding to snapshot l . Since an active sensor influences $N = 2B/D$ snapshots, we see from Fig. 2 that Z_l contains contributions from the desired signal (plus noise) for $|l| \leq N/2$, and contains contributions from noise only for $|l| > N/2$. The azimuth estimate is given by

$$\hat{l} = \arg \max_l Y_l$$

where

$$Y_l = \sum_{k=l-\frac{N}{2}}^{l+\frac{N}{2}} Z_k \quad (20)$$

is the accumulation of the snapshot statistics over a beamwidth centered around a hypothesized bin l (For simplicity, we make a slight change in notation, assuming that the normalized beamwidth, or the number of snapshots affected by a sensor, is $N + 1$, where N is even. The mean squared error thus derived is actually an upper bound for the case when the normalized beamwidth is N .) Since bin 0 is the correct bin, the azimuth error if bin l is chosen is lD . The mean squared azimuth

localization error due to choosing the wrong bin can therefore be written as

$$E[(\hat{l} - 0)D]^2 = E[|\hat{l}|^2]D^2.$$

We have

$$E[|\hat{l}|^2] = \sum_k k^2 p_k \quad (21)$$

where

$$p_k = P[\text{choose bin } k] = P[k = \arg \max_l Y_l]$$

is the probability that bin k has the maximum accumulated statistic. Since the probability of attaining a maximum for an accumulated statistic containing noise-only snapshot statistics is very small, we limit the summation in (22) for $|k| \leq N/2$ (for $|k| > N/2$, Y_k has contributions from noise alone). Thus, we wish to evaluate

$$E[|\hat{l}|^2] = \sum_{k=-N/2}^{N/2} k^2 p_k = 2 \sum_{k=1}^{N/2} k^2 p_k \quad (22)$$

by symmetry. For $k \neq 0$, we can bound p_k by using pairwise comparison with the accumulated statistic corresponding to the correct bin 0 as follows:

$$\begin{aligned} p_k &\leq P_k = P[Y_k > Y_0] \\ &= P\left[Z_{N/2+1} + \dots + Z_{N/2+k} > Z_{-N/2} + \dots + Z_{k-1-N/2}\right]. \end{aligned} \quad (23)$$

Note that $Z_{N/2+1} + \dots + Z_{N/2+k}$ is a sum of k snapshot statistics containing contributions from noise alone, while $Z_{-N/2} + \dots + Z_{k-1-N/2}$ is a sum of k snapshot statistics containing signal as well as noise contributions. Under our model, the received signal in the l th snapshot is of the form

$$r_l(t) = s(t - \tau)e^{j\theta_l} + n_l(t)$$

signal present: sensor falls in beam.

In what follows, we label snapshot statistics corresponding to this ‘‘signal-present’’ scenario as $Z_l^{(s)}$.

$$r_l(t) = n_l(t)$$

noise only: sensor does not fall in beam.

We label snapshot statistics corresponding to this ‘‘noise-only’’ scenario as $Z_l^{(n)}$. Note that the WGN processes n_l are independent for different l , so that the snapshot statistics (conditioned on the sensor location) are independent random variables. Under these assumptions, it is easy to see from (19) that $Z_l^{(s)}$ are i.i.d. Rician random variables for ‘‘signal-present’’ snapshots, while $Z_l^{(n)}$ are i.i.d. Rayleigh random variables for ‘‘noise-only’’ snapshots.

Since the azimuth error scales with D , a convenient normalization factor along the y direction is $m_y = D$. Defining the normalized azimuth coordinate $Y = y/m_y$, we infer from the preceding that (ignoring the bin quantization error)

$$\sigma_Y^2 \leq 2 \sum_{k=1}^{N/2} k^2 P_k \quad (24)$$

where P_k , defined in (23), is rewritten below to emphasize the dependence on the presence or absence of a signal

$$P_k = P\left[Z_{N/2+1}^{(n)} + \dots + Z_{N/2+k}^{(n)} > Z_{-N/2}^{(s)} + \dots + Z_{k-1-N/2}^{(s)}\right].$$

It remains to compute P_k . Computer simulations are a straightforward means of estimating P_k , since the values of k being considered are not very large. For moderately large k , an accurate alternative to computer simulations is the central limit theorem (CLT): since $Z_l^{(s)}, Z_l^{(n)}$ are independent random variables, the random variable $U_k = (Z_{N/2+1}^{(n)} + \dots + Z_{N/2+k}^{(n)}) - (Z_{-N/2}^{(s)} + \dots + Z_{k-1-N/2}^{(s)})$ can be approximated as a Gaussian random variable with the same mean and variance. Define μ_s, σ_s^2 as the mean and variance of $Z_l^{(s)}$, respectively, and μ_n, σ_n^2 as the mean and variance of $Z_l^{(n)}$, respectively. (The dependence of these parameters on SNR has been suppressed from the notation.) Then

$$E[U_k] = k(\mu_n - \mu_s), \quad \text{Var}(U_k) = k(\sigma_n^2 + \sigma_s^2)$$

and

$$\begin{aligned} P_k &= P[U_k > 0] \\ &\approx Q\left(\frac{\sqrt{k}|\mu_s - \mu_n|}{\sqrt{(\sigma_s^2 + \sigma_n^2)}}\right) \quad \text{CLT approximation.} \end{aligned}$$

In our computations, we use computer simulations for estimating P_k for $k \leq 5$, and the CLT approximation for $k > 5$. An alternative approach is to employ a Chernoff bound for P_k , but we find it to be less accurate than the method employed.

Since $\{P_k\}$ decay with SNR, so does the variance σ_Y^2 . However, P_k also decays exponentially with k , as evident from the CLT approximation, as well as from a Chernoff bound analysis. Thus, the first few terms dominate in the summation on the RHS of (24). Since the beamwidth of the antenna only affects the number of terms being summed, the azimuth localization error variance is expected to be insensitive to the beamwidth.

D. Tradeoffs Between Parameters

In this section, ML localization performance is studied with emphasis on tradeoffs between SNR, signal bandwidth, antenna beamwidth, and antenna beamshape. A single active sensor is localized using the algorithm in Section III-A using the normalized rms error (obtained from scale-invariant quantities) as the performance metric. However, the absolute rms errors are also shown on an alternate y axis in the plots. Due to the proportional relationship between antenna beamwidth and N (the number of times the sensor is illuminated), the two terms are used interchangeably, while the results are presented in terms of N . The

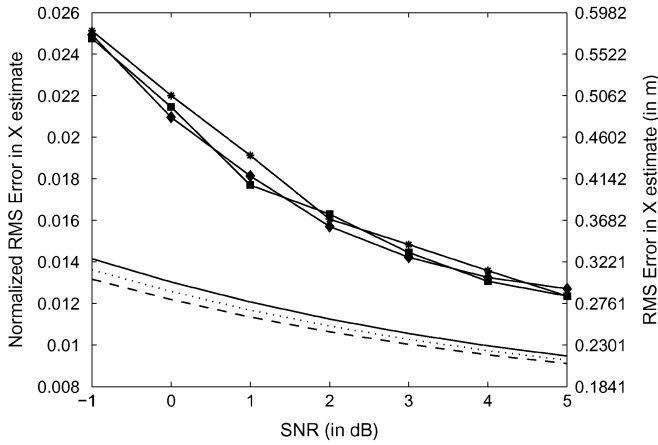


Fig. 3. RMS estimation error in the range estimate versus SNR for different values of beamwidth: The rms error in scale-invariant units and in meters are shown on the 2 y axes.

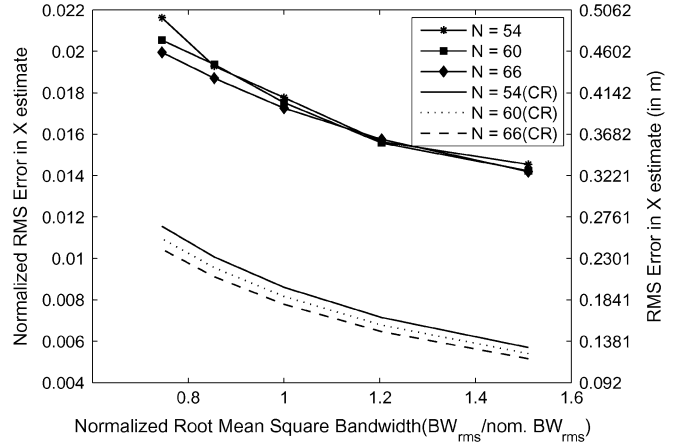


Fig. 5. RMS estimation error in the range estimate versus normalized rms bandwidth for different values of beamwidth: The rms error in scale-invariant units and in meters are shown on the two y axes.

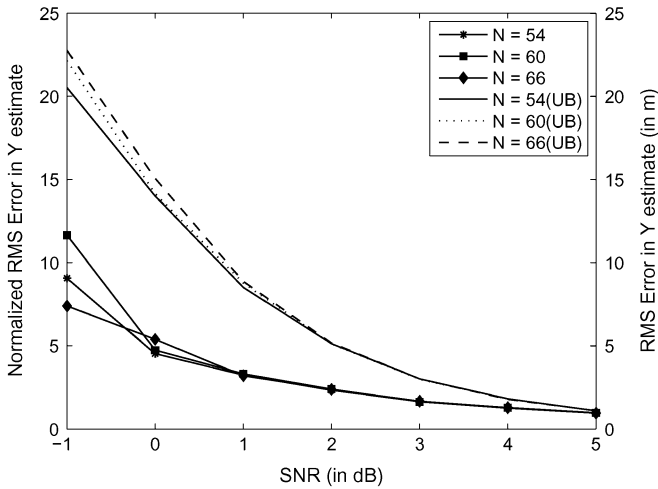


Fig. 4. RMS estimation error in the azimuth estimate versus SNR for different values of beamwidth: The rms error in scale-invariant units and in meters are shown on the two y axes.

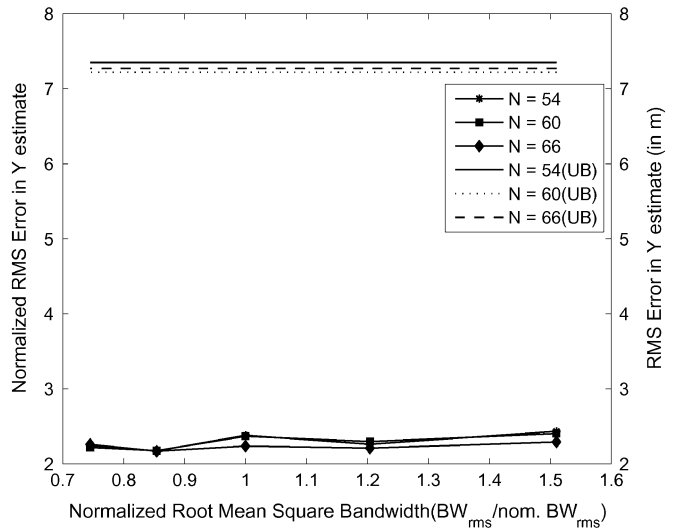


Fig. 6. RMS estimation error in the azimuth estimate versus normalized rms bandwidth for different values of beamwidth: The rms error in scale-invariant units and in meters are shown on the two y axes.

nominal values defined in Section II-D were used for any parameter not explicitly mentioned in the simulation results.

1) *Effect of SNR:* In Figs. 3 and 4, the simulated rms estimation error in the range and azimuth coordinates are plotted against SNR. The CRLB for the x estimate and union bound (UB) for the y estimate are also plotted for comparison. The bounds predict the trends in the error variance accurately, confirming the insights gained from the analysis in Sections IV-B and IV-C. The rms estimation error in both the range and azimuth coordinates decrease with SNR, and the analysis accurately predicts the expected performance improvement with SNR. Since delay estimation is asymptotically efficient, the rms error is expected to achieve the CRLB at high SNR. However, we observe a gap to the CRLB in the simulations, which can be attributed to two main factors. First, the validity of the approximation error (4) becomes progressively worse as the beamwidth is increased. In the far-field approximation (3), the effect of the range on the azimuth coordinate of the sensor is neglected. At the nominal range $R = 3000$ m and beamwidth

$2B = 60$ m, the worst case error due to the approximation is $B^2/2R = 0.148$ m, using (4) and recalling that the range estimate is the speed of light times half the round trip time. Second, our localization algorithm finds the range bin closest to the true sensor range at high SNR, which leads to residual quantization error. While this quantization error can be essentially eliminated by interpolation, we do not attempt to do this here. Instead, we note that the quantization and approximation errors do account for the gap to the CRLB for our system. For the system parameters in Section II-D, the quantization interval is $\Delta = 0.578$ m, and leads to a quantization error variance of $\Delta^2/12 = 0.0278$ m². According to Fig. 3, at 5 dB SNR, the observed mean squared error is 0.0808 m² and CRLB is 0.0455 m². The gap to the CRLB is 0.0353 m² which is well approximated by the sum of the quantization and approximation errors as $0.0278 + 0.0217 = 0.0495$ m².

2) *Effect of Signal Bandwidth:* In Figs. 5 and 6, the rms estimation error in the range and azimuth coordinates is plotted versus the normalized rms bandwidth of the transmitted signal

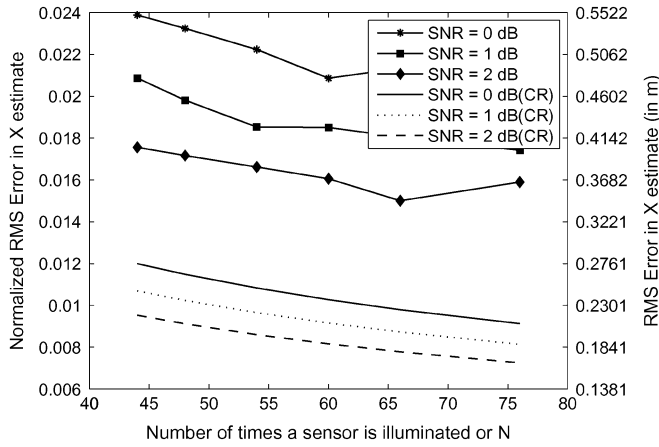


Fig. 7. RMS estimation error in the range estimate versus beamwidth for different values of SNR: The rms error in scale-invariant units and in meters are shown on the two y axes.

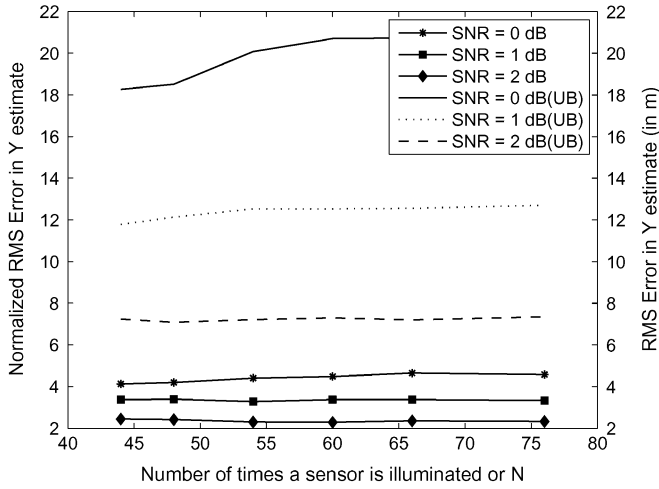


Fig. 8. RMS estimation error in the azimuth estimate versus beamwidth for different values of SNR: The rms error in scale-invariant units and in meters are shown on the two y axes.

for different values of N at $\text{SNR} = 2$ dB. The normalized bandwidth is the ratio of the true bandwidth and nominal bandwidth as defined in Section IV-B. The range estimate is inversely proportional to the rms bandwidth of the transmitted signal. This is reflected in Fig. 5, which shows the rms error decreasing with the bandwidth and closely matches the CRLB in trend. On the other hand, the azimuth estimate is independent of the signal bandwidth and determined solely by the SNR. The agreement in trend between the estimation error in the y coordinate and analytic results in Fig. 6 also validates this analysis.

3) *Effect of Antenna Beamwidth:* According to the CRLB, the effective SNR for range estimation increases with N due to noise averaging over multiple snapshots, thereby improving performance. On the other hand for azimuth estimation, the error variances are dependent strongly on the SNR and weakly on N . The azimuth resolution is expected to be fairly insensitive to changes in antenna beamwidth. Figs. 7 and 8, show the rms estimation in the range and azimuth coordinates versus N for different values of SNR along with the analytical bounds, verifying that the dependence on the beamwidth is as expected.

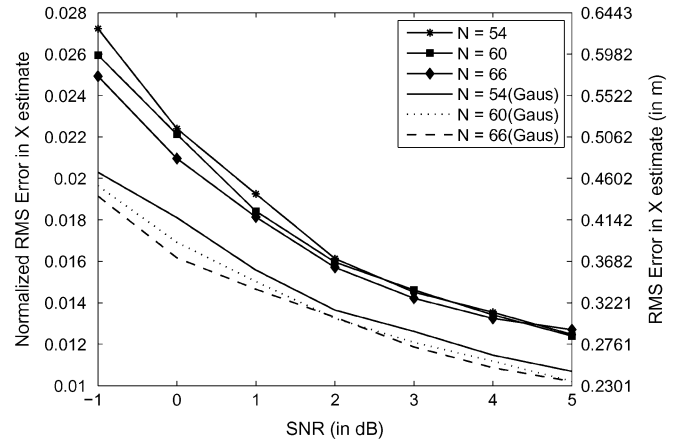


Fig. 9. RMS estimation error in the range estimate versus SNR for different values of beamwidth for rectangular and Gaussian beams: The rms error in scale-invariant units and in meters are shown on the two y axes.

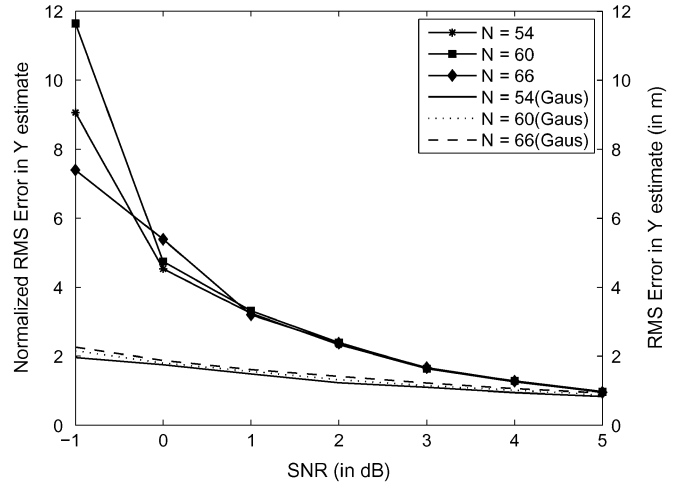


Fig. 10. RMS estimation error in the azimuth estimate versus SNR for different values of beamwidth for rectangular and Gaussian beams: The rms error in scale-invariant units and in meters are shown on the two y axes.

4) *Effect of Antenna Beam Shape:* In Figs. 9 and 10, the performance of a more realistic, smooth Gaussian beam, defined in Section II-B, is compared against the idealized rectangular beam to gain insight into the effect of antenna beamshape. The Gaussian beams approximate the beamshape of parabolic antennae in the far-field fairly well. The beamwidth N of the rectangular and Gaussian beams are maintained equal, and the beamshapes are normalized so that the received power at the collector from each sensor is NP_s in order to isolate the effect of the beamshape. The Gaussian beam performs significantly better, and its better performance along the azimuth direction can be explained by the following two observations. First, the Gaussian beam has better autocorrelation properties (sharper autocorrelation peak) than the rectangular beam. Second, with the rectangular beam when the y coordinate of a sensor lies between snapshots j and $j + 1$, the received signal at the collector is exactly the same in the absence of noise, and this ambiguity causes performance degradation. On the contrary, with the Gaussian beam since the received power at various snapshots is a function of the sensor location, each location has a distinct

received signal in the absence of noise, which leads to better performance. The improvement in the range estimate is mainly due to the improvement in the azimuth estimate. Although the algorithm is designed assuming that the range and azimuth estimate are decoupled [due to (3)], in reality they are not. This result also justifies the study of the performance of the rectangular beamshape as a worst case scenario and an upperbound on performance in a practical setup.

V. PERFORMANCE WITH INTERSENSOR INTERFERENCE

We now evaluate the performance of the decision-directed localization algorithm in Section III-B. We first establish a termination criterion for the algorithm based on our analysis of noise-limited performance. The performance of the decision-directed algorithm and the optimal joint ML localization are compared for a small two-sensor example (the joint ML algorithm is too computationally complex for a larger number of sensors). There is a moderate penalty due to the loss of optimality, but this appears to be unavoidable, given the complexity of the jointly optimal algorithm. Finally, we evaluate the performance of the decision-directed algorithm for a dense sensor deployment.

For dense deployments, intersensor interference can cause significant degradation in detection performance. On the other hand, sensors that are close enough to interfere with each other may have correlated observations, and it may suffice to localize a subset of active sensors within such a cluster. This motivates us to define the concept of detection radius R_d : if the localization algorithm detects a sensor at a given location X , then it is deemed to have been successful in localizing any active sensor within a radius R_d of X . In practice, one might set R_d based on the anticipated spatial correlation in the sensor readings. Thus, a *miss* occurs if the decision statistics for *all* locations within radius R_d of an active sensor are below a threshold. A *false alarm* occurs at a specific location if its decision statistic exceeds the threshold, and it is not within R_d of an active sensor. In our numerical results, the sensors are deployed using a uniform distribution to achieve a density of 1 m^{-2} and R_d is measured in meters. In Section V-A, where we determine the threshold based on a noise-limited analysis, we choose a small value of $R_d = 0.5$. In Section V-C, where we investigate interference-limited performance for dense deployment, we consider the effect of increasing R_d on the probability of miss, in order to understand how correlations between sensor observations can ease the task of localization.

A. Termination Criterion for Decision-Directed Algorithm

We now describe a method to choose a threshold to terminate the sequential detection algorithm in Section III-B, when it is used to localize an unknown number of sensors. Under the detection algorithm, we repeatedly search for maxima in the decision statistic (16) until the magnitude of the maximum is below a threshold. It is difficult to analyze the effect of uncancelled interference on the performance of the decision-directed algorithm, hence we set the threshold based on noise-limited performance (i.e., it suffices to consider a single active sensor when determining the threshold). Letting p_{miss} denote the probability of miss, and p_{fa} denote the probability of a false alarm,

the tradeoff between p_{miss} and p_{fa} is characterized by the receiver operating characteristic (ROC), which plots p_{miss} versus p_{fa} along a curve parameterized by the threshold. We use this curve to read off the threshold corresponding to desired levels of miss and false alarm probabilities.

Receiver Operating Characteristic (ROC): We use the notation defined in Section IV-C, and compare the accumulated statistics Y_l versus a threshold T . Suppose that there is an active sensor at bin 0, and suppose that bins $l \in L$ are within radius R_d of bin 0. A miss occurs if $Y_l < T$ for all $l \in L$. We obtain an upper bound on the probability of miss as follows:

$$p_{\text{miss}} = P(\max_{l \in L} Y_l < T) \leq P(Y_0 < T)$$

Recall that $Y_0 = \sum_{l=-N/2}^{N/2} Z_l^{(s)}$ (for a normalized beamwidth of $N + 1$), where $Z_l^{(s)}$ are i.i.d Rician random variables, each with mean μ_s and variance σ_s^2 . Thus, for moderately large N , Y_0 can be approximated as a Gaussian random variable with the mean $(N + 1)\mu_s$ and variance $(N + 1)\sigma_s^2$. Replacing $N + 1$ by N for notational convenience, we obtain the following approximation for p_{miss} :

$$p_{\text{miss}} \leq P(Y_0 < T) \approx Q\left(\frac{N\mu_s - T}{\sqrt{N}\sigma_s}\right) \quad \text{CLT approximation.} \quad (25)$$

We now compute an approximation to p_{fa} , assuming that active sensors have been detected and cancelled. In this case, the accumulated decision statistic Y_k at a location k which is not within R_d of an active sensor is a sum of decision statistics due to “noise-only” snapshots: $Y_k = \sum_{l=k-N/2}^{k+N/2} Z_l^{(n)}$. Under a central limit theorem approximation, and replacing $N + 1$ by N for notational convenience as before, we obtain that

$$p_{\text{fa}} = P(Y_k > T) \approx Q\left(\frac{T - N\mu_n}{\sqrt{N}\sigma_n}\right). \quad (26)$$

The parameters μ_s, μ_n, σ_s , and σ_n , which determine the ROC, depend on the operating SNR alone, apart from an arbitrary scale factor (if both signal and noise are scaled by a factor a , then all of the preceding parameters, as well as the threshold T , scale by a , but the SNR and ROC remains unchanged). Fig. 11 shows the ROC for several values of SNR. The ROC is parametrized by the threshold T : increasing the threshold increases p_{miss} and decreases p_{fa} , and vice-versa when decreasing the threshold. The operating point, in terms of SNR and threshold, is determined by user-defined tolerances for miss and false alarm. While p_{fa} is the probability of false alarm at a given location, what is experienced by the user is the false alarm rate (FAR), defined as the probability that there is a false alarm at *some* location which is not within R_d of an active sensor. If there are M_{cand} candidate locations in our discrete grid, a union bound on the FAR is given by

$$\text{FAR} \leq p_{\text{fa}} M_{\text{cand}}. \quad (27)$$

Example choice of threshold: Consider user-defined tolerances for the probability of miss and the false alarm rate as follows: $p_{\text{miss}} \leq 10^{-2}$ and $\text{FAR} \leq 10^{-1}$. The sensor field is discretized into $M_{\text{cand}} = 500000$ candidate locations for running

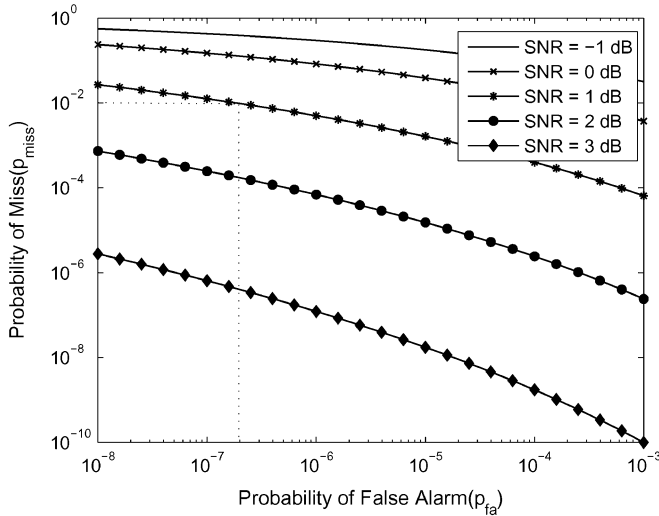


Fig. 11. Receiver Operational Characteristic: p_{miss} versus p_{fa} for different values of SNR under the noise-limited setting.

the localization algorithm, so that the requirement on FAR translates to $p_{\text{fa}} \leq \text{FAR}/M_{\text{cand}} = 2 \times 10^{-7}$. From the ROC, the operating point must lie within the area enclosed by the dotted lines, and this provides the minimum operating SNR = 2 dB. To achieve the desired $p_{\text{miss}} = 10^{-2}$, at this operating SNR of 2 dB (since energy is at a premium, the lowest possible SNR is chosen), a threshold T is chosen using (25). This threshold and operating SNR are used to study performance of the suboptimal scheme in Section V-C.

While we have used upper bounds on p_{miss} and FAR in the preceding formulation, this is still not sufficient to offset the effect of intersensor interference for a dense deployment. Thus, in practice, it would be necessary to add a link margin to the operating SNR determined by the ROC above.

B. Suboptimal Algorithm Versus Optimal ML Localization

The suboptimal detection procedure in Section III.B for multiple sensor localization was adopted due to the computational complexity of the optimal ML algorithm. In Fig. 12, the performance of this suboptimal algorithm is compared against the optimal algorithm for the simple instance of two active sensors in the field (when the optimal algorithm is still computationally tractable). The rms estimation error in the azimuth coordinate is plotted against SNR for the two algorithms. When there is no overlap between the received signals corresponding to the two sensors in either the range or azimuth directions, then there is no intersensor interference. In this case, the suboptimal and optimal algorithms are identical and have the same performance. Furthermore in our examples, the bandwidth of the transmitted signal is large enough to provide adequate resolution in the range (or x) direction. Hence, to study the effect of intersensor interference, we focus on the scenarios where the two sensors have the same x coordinate and are closely enough spaced in the y direction to cause interference.

The simulations were performed on the system described in Section II-D with all parameters at their nominal values. In Fig. 12, the rms azimuth estimation error in scale invariant units is plotted versus SNR for the two algorithms. As expected, the

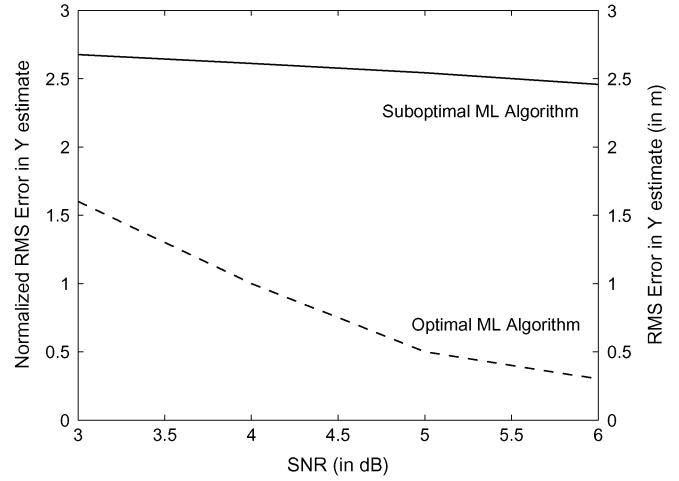


Fig. 12. RMS estimation error in the azimuth coordinate versus SNR for the suboptimal and optimal ML algorithms with two active sensors.

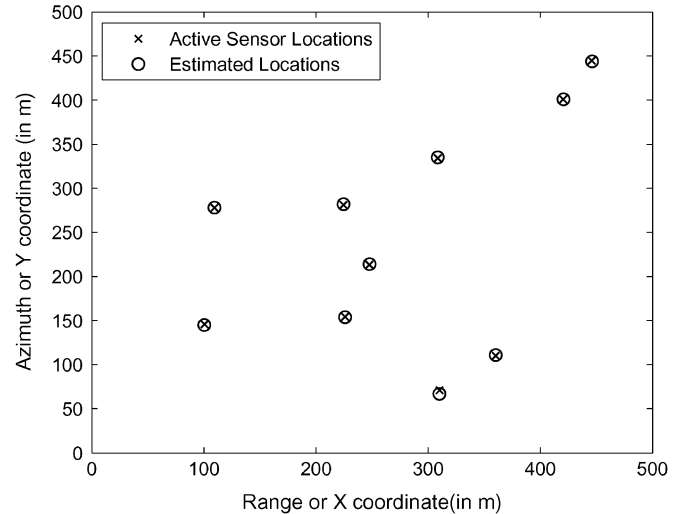


Fig. 13. Detection and localization performance of suboptimal algorithm for 10 active sensors: The plot shows the 500 m \times 500 m sensor field with true and estimated sensor locations.

optimal ML algorithm performs much better and the disparity increases with SNR. However, at SNR = 4 dB the performance loss is about 1 unit, which is acceptable, considering that the computational complexity of the optimal algorithm is many orders of magnitude larger. As with a single sensor, the performance for both algorithms improves with SNR. In Figs. 13 and 14, two instances of multiple sensor detection and localization using the suboptimal algorithm are presented at SNR = 4 dB such that $p_{\text{miss}} = 10^{-2}$ and $p_{\text{fa}} = 2 \times 10^{-8}$ (false alarm rate of 10^{-2}).

C. Simulation Results for Dense Sensor Deployment

In this section, we investigate the algorithm performance in dense deployments, such as the scenario with 50 active sensors depicted in Fig. 14. In such scenarios, we find through our simulations that a significant subset of active sensors are not detected, either due to destructive interference between the responses of nearby sensors (this is found to be the dominant effect in our simulations), or due to imperfect cancellation of the responses

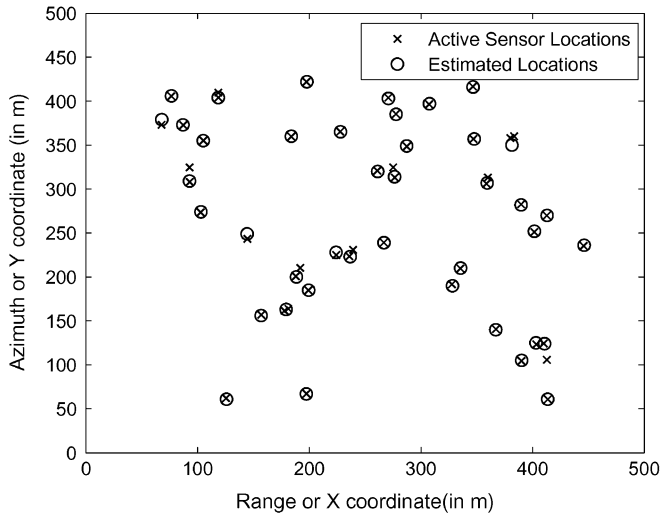


Fig. 14. Detection and localization performance of suboptimal algorithm for 50 active sensors: The plot shows the 500 m \times 500 m sensor field with true and estimated sensor locations.

TABLE I
PROBABILITY OF MISS DECREASES SIGNIFICANTLY
WITH DETECTION RADIUS R_d

No. of Sensors	$R_d = 1$ m	$R_d = 2$ m	$R_d = 3$ m
10	0.0254	0.0270	0.0151
50	0.1168	0.0518	0.0143
100	0.1818	0.0719	0.0138

of the detected sensors. As aforementioned, it may be acceptable to detect a subset of the active sensors in a cluster if their observations are spatially correlated. We, therefore, explore the influence of the detection radius R_d on the probability of miss, as shown in the simulation results presented in Table I. While we are interested in miss probabilities of the order of 1%–10%, the threshold is chosen based on a noise-limited analysis for $p_{\text{miss}} = 10^{-3}$ in order to provision for the additional intersensor interference. From Table I, we see that spatial correlation can significantly simplify localization, noting the significant reduction in p_{miss} as we increase R_d . For $R_d = 1, 2$ m, the observed p_{miss} increases with the number of sensors due to increase in the interference. However, for $R_d = 3$ m, the p_{miss} decreases marginally with the number of sensors, since $R_d = 3$ m is large enough that some undetected non-interfering sensors randomly fall within R_d of a detected sensor, thus increasing our count of the number of “detected” sensors. For instance, two sensors located about 3 m apart in the range direction do not interfere with each other. However, if one sensor went undetected due to noise alone, for $R_d = 3$ m, this sensor would be denoted as being detected, reducing the observed p_{miss} .

VI. CONCLUSION

We have shown, using an idealized model, that accurate localization is possible in large-scale imaging sensor nets with “dumb,” severely energy-constrained, sensor nodes. However, a far more detailed design is required for translating the promise of these ideas into practice. This is the subject of our current efforts in design and implementation of a prototype imaging

sensor net [6], [7], in which the sensors electronically reflect a spread spectrum beacon emitted by the collector, while superimposing a frequency shift (to avoid backscatter) and low-rate data modulation on it. Since the modulation imposed by the sensors on the beacon is slow compared to the chip rate, localization algorithms can be developed ignoring data modulation, as in the simple model employed in this paper. The localization algorithms must also be modified to allow for the stationary collector nodes to be employed in the prototype, but this is a straightforward extension [32] of the techniques in the present paper. The major open issues related to implementation correspond to hardware development and baseband processing.

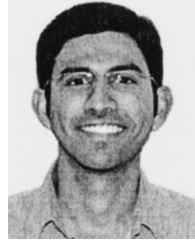
Open theoretical issues include performance scaling with sensor density, modeling and tracking of events, and Bayesian approaches to localization. Methods for compressing and representing data for efficient recovery via an imaging sensor net are also important topics for future investigation.

REFERENCES

- [1] P. Gupta and P. Kumar, “The capacity of wireless networks,” *IEEE Trans. Inf. Theory*, vol. 46, no. 2, pp. 388–404, 2000.
- [2] S. Toumpis and A. Goldsmith, “Capacity regions for wireless ad hoc networks,” *IEEE Trans. Wireless Commun.*, vol. 2, no. 4, pp. 736–748, 2003.
- [3] F. Xue, L.-L. Xie, and P. Kumar, “The transport capacity of wireless networks over fading channels,” in *Proc. 2004 Int. Symp. Inf. Theory (ISIT 2004)*, 2004, pp. 372–372.
- [4] A. Jovicic, P. Viswanath, and S. Kulkarni, “Upper bounds to transport capacity of wireless networks,” *IEEE Trans. Inf. Theory*, vol. 50, no. 11, pp. 2555–2565, 2004.
- [5] O. Leveque and E. Telatar, “Information theoretic upper bounds on the capacity of large extended ad hoc wireless networks,” in *Proc. 2004 Int. Symp. Inf. Theory (ISIT 2004)*, 2004, pp. 370–370.
- [6] B. Ananthasubramaniam, R. Mudumbai, and U. Madhow, “New communication paradigms for very large-scale sensor networks,” in *Inf. Process. Sens. Netw. (IPSN’05)*, 2005 [Online]. Available: http://www.ee.ucla.edu/mbs/ipsn05/wip/05_BAnanthasubramaniam_abstract.pdf
- [7] U. Madhow, M. J. W. Rodwell, B. Ananthasubramaniam, M. K. Seo, and P. Park, “Imaging sensor nets: An rfid-inspired framework for million node sensor networks,” in *Book of Extended Abstracts, International Workshop on RFID and Wireless Sensors*, Kanpur, India, Nov. 2005, pp. 32–33 [Online]. Available: http://www.iitk.ac.in/ee/RFIDWS/rfweb/Book_of_Extended_Abstracts_Final.pdf, [online] Available
- [8] D. C. Munson and R. L. Visentin, “A signal processing view of strip-mapping synthetic aperture radar,” *IEEE Trans. Acoust., Speech, Signal Process.*, vol. 37, no. 12, pp. 2131–2147, Dec. 1989.
- [9] J. A. C. Lee, O. Arikan, and D. C. Munson, “Formulation of a general imaging algorithm for high resolution synthetic aperture radar,” in *Proc. IEEE Int. Conf. Acoust., Speech, Signal Process.*, 1996, vol. 4, pp. 2092–5.
- [10] J. C. Curlander and R. N. McDonough, *Synthetic Aperture Radar: Systems and Signal Processing*. New York: Wiley, 1991.
- [11] B. Ananthasubramaniam and U. Madhow, “Virtual radar imaging for sensor networks,” in *Proc. 3rd Int. Symp. Inf. Process. Sens. Netw.*, Berkeley, CA, USA, Apr. 2004, pp. 294–300, ACM Press, New York.
- [12] R. E. Blahut, *Theory of Remote Image Formation*. Cambridge: Cambridge Univ. Press, 2004.
- [13] D. C. Munson, J. D. O’Brien, and W. K. Jenkins, “A tomographic formulation of spotlight-mode synthetic aperture radar,” in *Proc. IEEE*, 1983, vol. 71, no. 8, p. 917, 925.
- [14] B. Ananthasubramaniam and U. Madhow, “Virtual radar approach to event localization in sensor networks,” in *Proc. Int. Symp. Inf. Theory (ISIT 2004)*, Chicago, IL, Jun. 2004, p. 517.
- [15] R. Stoleru, T. He, J. A. Stankovic, and D. Luebke, “A high-accuracy, low-cost localization system for wireless sensor networks,” in *Proc. ACM Sensys 2005*, 2005, pp. 13–26.
- [16] L. Doherty, K. S. Pister, and L. E. Ghaoui, “Convex position estimation in wireless sensor networks,” in *Proc. IEEE INFOCOM 2001*, Anchorage, AK, Apr. 2001, vol. 3, pp. 1655–1663.

- [17] A. Savvides, C.-C. Han, and M. B. Srivastava, "Dynamic fine-grained localization in ad-hoc networks of sensors," in *Proc. Mobile Computing and Netw. (MOBICOM 2001)*, Jul. 2001, pp. 166–179.
- [18] A. Savvides, H. Park, and M. Srivastava, "The bits and flops of the n-hop multilateration primitive for node localization problems," in *Proc. 1st ACM Int. Workshop on Wireless Sens. Netw. Applicat.*, Atlanta, GA, Sep. 2002, pp. 112–121.
- [19] D. Niculescu and B. Nath, "Ad hoc positioning system (APS)," in *Proc. IEEE GLOBECOM 2001*, San Antonio, TX, Nov. 2001, vol. 5, pp. 2926–2931.
- [20] C. Savarese, J. Rabay, and K. Langendoen, "Robust positioning algorithms for distributed ad-hoc wireless sensor networks," in *Proc. USENIX Tech. Ann. Conf.*, Monterey, CA, Jun. 2002, pp. 317–327.
- [21] N. Bulusu, J. Heidemann, D. Estrin, and T. Tran, "Self-configuring localization systems: Design and experimental evaluation," *ACM Trans. Embedded Comput. Syst.*, vol. 3, no. 1, pp. 24–60, 2004.
- [22] N. Priyantha, H. Balakrishnan, E. Demaine, and S. Teller, "Anchor-free distributed localization in sensor networks Tech. Rep. TR-892, Apr. 2003, MIT LCS.
- [23] C. Intanagonwivat, R. Govindan, and D. Estrin, "Directed diffusion: A scalable and robust communication paradigm for sensor networks," in *Proc. ACM/IEEE Int. Conf. Mobile Comput. Netw. (Mobicom)*, Aug. 2000, pp. 56–57.
- [24] J. Liu, D. Petrovic, and F. Zhao, "Multi-step information-directed sensor querying in distributed sensor network," in *Proc. Int. Conf. Acoust., Speech Signal Process. (ICASSP'03)*, Hong Kong, China, Apr. 2003, vol. 5, pp. 145–148.
- [25] B. Krishnamachari, Y. Mourtada, and S. Wicker, "The energy robustness tradeoff for routing in wireless sensor networks," in *Proc. IEEE Int. Conf. Commun. (ICC'03)*, Anchorage, AK, May 2003, vol. 3, pp. 1833–7.
- [26] W. R. Heinzelman, A. Chandrakasan, and H. Balakrishnan, "Energy-efficient communication protocol for wireless microsensor networks," in *HICSS'00: Proc. 33rd Hawaii Int. Conf. Syst. Sci.*, 2000, vol. 8, p. 8020, IEEE Comp. Soc..
- [27] S. S. Pradhan, J. Kusuma, and K. Ramchandran, "Distributed compression in a dense microsensor network," *IEEE Signal Process. Mag.*, vol. 19, pp. 51–60, Mar. 2002.
- [28] S. S. Pradhan and K. Ramchandran, "Distributed source coding using syndromes (Discus): Design and construction," *IEEE Trans. Inf. Theory*, vol. 49, no. 3, pp. 51–60, Mar. 2003.
- [29] S. D. Servetto, "Distributed signal processing algorithms for the sensor broadcast problem," in *Proc. Ann. Conf. Inf. Sci. Syst. (CISS)*, Mar. 2003.
- [30] M. A. Paskin, C. Guestrin, and J. McFadden, "A robust architecture for distributed inference in sensor networks," in *Proc. Inf. Process. Sens. Netw., (IPSN'05)*, 2005, pp. 55–62.
- [31] A. Scaglione and S. D. Servetto, "On the interdependence of routing and data compression in multi-hop sensor networks," in *Proc. ACM Int. Conf. Mobile Comput. Netw. (Mobicom)*, Sep. 2002, pp. 140–147.

- [32] B. Ananthasubramaniam and U. Madhow, "Detection and localization in large scale sensor networks," in *Proc. Int. Symp. Inf. Theory (ISIT 2005)*, Adelaide, Australia, Sep. 2005, pp. 517–0.
- [33] H. V. Poor, *An Introduction to Signal Detection and Estimation*, 2nd ed. New York: Springer, 2005.



Bharath Ananthasubramaniam (S'02) received the Bachelor's degree in electrical engineering from the Indian Institute of Technology, Madras, in 2002 and the M.S. degree in electrical engineering from the University of California, Santa Barbara, in 2004. He is currently pursuing the Ph.D. degree at the Department of Electrical and Computer Engineering, University of California, Santa Barbara.

His research interests are in physical layer design of wireless networks, communication architectures for wireless sensor networks and millimeter-wave wireless systems with a focus on hardware constrained algorithm design.



Upamanyu Madhow (S'86–M'90–SM'96–F'05) received the Bachelor's degree in electrical engineering from the Indian Institute of Technology, Kanpur, in 1985 and the M.S. and Ph.D. degrees in electrical engineering from the University of Illinois, Urbana-Champaign, in 1987 and 1990, respectively.

From 1990 to 1991, he was a Visiting Assistant Professor at the University of Illinois. From 1991 to 1994, he was a Research Scientist at Bell Communications Research, Morristown, NJ. From 1994 to 1999, he was on the faculty of the Department of Electrical and Computer Engineering at the University of Illinois, Urbana-Champaign. Since December 1999, he has been with the Department of Electrical and Computer Engineering at the University of California, Santa Barbara, where he is currently a Professor. His research interests are in communication systems and networking, with current emphasis on wireless communication, sensor networks and multimedia security.

Dr. Madhow is a recipient of the NSF CAREER award. He has served as Associate Editor for Spread Spectrum for the IEEE TRANSACTIONS ON COMMUNICATIONS, and as Associate Editor for Detection and Estimation for the IEEE TRANSACTIONS ON INFORMATION THEORY. He currently serves as Associate Editor for the IEEE TRANSACTIONS ON INFORMATION FORENSICS AND SECURITY.